Hot Wire / Hot Film
Paper 21

ROTATING HOT-WIRE MEASUREMENTS IN A MODEL TURBINE STAGE

C.D. Sheldrake, R.W. Ainsworth

Deptartment of Engineering Science
University of Oxford
Oxford OX1 3PJ

Rotating Hot-Wire Measurements In A Model Turbine Stage

C.D. Sheldrake, R.W. Ainsworth
Department of Engineering Science
University of Oxford

Abstract

This paper describes the use of rotating hot-wires for making two-dimensional aerodynamic measurements in a model gas turbine facility at Oxford (**Ainsworth, *et al*, 1988**). The technique provides a direct measurement, at high bandwidth, of the pitch-wise variation in the turbine inlet Mach number and inlet whirl angle.

A single sensor hot-wire probe has already been used successfully to determine the magnitude of the flow vector entering the turbine, in the rotor relative frame of reference (**Sheldrake and Ainsworth, 1994**). Using a similar technique, a miniature two sensor hot-wire probe, of the conventional *X*-array configuration, has been mounted at mid-height into the leading edge of a turbine blade. The temperature of the probe's sensing elements are controlled by a high frequency response anemometer circuit contained within the turbine shaft, such that both the hot-wire probe and the anemometer module rotate together, in the same frame of reference.

The dual sensor hot-wire probe is calibrated for velocity *in situ*, using a compact calibration nozzle mounted inside the working section of the turbine facility. The angular response of the probe is characterised by determining two yaw coefficients, using the effective cooling velocity concept (**Jorgensen, 1971**). The results from the yaw and velocity calibrations are then combined to provide a complete two-dimensional probe calibration.

The high bandwidth results obtained from a rotor relative inlet survey using the single and dual sensor probe are presented and compared with a CFD prediction generated by the unsteady viscous solver UNSFLO.

Nomenclature

A, B	Constants
E	Output voltage
k	Pitch Factor
n	Exponent
U	Normal velocity component
V	Tangential velocity component
$\tilde{V}$	Magnitude of velocity
V_{eff}	Effective cooling velocity
α	Flow yaw angle
$\bar{\alpha}$	Hot-wire separation angle
θ	Flow angle

Subscripts

tip	Tip
root	Root
w	Wire
θ	Angle

Introduction

The Oxford Rotor facility (**Ainsworth, *et al*, 1988**) has been built to provide a simulation of the conditions encountered in a modern rotating gas turbine stage. Using this facility an understanding of the complex flow phenomena within the stage may be gained, and valuable data acquired for comparison with computational fluid dynamic (CFD) predictions. The blade profile being tested in the Oxford rotor has been studied in a two-dimensional linear cascade (**Nicholson, 1981**) and as part of a simulated wake and shock passing experiment, using a rotating bar arrangement (**Doorly, 1985**). In the present experiment, a 0.62 scale model turbine stage incorporating highly instrumented turbine blades has been mounted as the working section in the Oxford Isentropic Light Piston Tunnel (ILPT).

The Rotor Facility

The Oxford Rotor facility consists of a single stage 0.5 m diameter shroudless turbine attached to an ILPT, Figure 1. The pump tube contains a light piston, which is driven forward by air delivered from a series of high pressure reservoirs, such that it compresses the air ahead of it. The compression process is approximately isentropic; when the desired total pressure is reached a fast-acting annular gate valve, contained within a bolster plate, is opened allowing high pressure air to enter the working section containing the turbine blade ring (60 blades) and nozzle guide vanes (36 blades).

The facility is able to simulate engine representative Mach and Reynolds numbers, as well as the relevant rotational groups. Details of the tunnel's operating point are shown below in Table 1.

Mass Flow Number $\frac{\dot{m}\sqrt{T_0}}{P_0}$	$7.04\text{x}10^{4}$ msK$^{1/2}$
Specific Speed $\frac{N}{\sqrt{T_0}}$	436 rpm/K$^{1/2}$
NGV Exit Mach Number	0.946
NGV Exit Reynolds Number	$2.7\text{x}10^{6}$
Upstream Total Pressure	$8.02\text{x}10^{5}$
Rotor Relative Exit Mach Number	0.959

Table 1

Tunnel monitoring consists of both fast and slow data acquisition. Throughout the 200 ms run time quasi-steady temperatures, pressures, and the turbine speed, are sampled at 434 Hz, this data being predominantly used to determine the turbine's operating point. Fast data is obtained around the design point for approximately 15 ms at a sample rate of 500 kHz. A copper loom on the turbine disc allows signals from blade mounted transducers to be taken to the stationary frame via a series of slip rings.

Blade Mounted Hot-wires and the "In-shaft" Anemometer Circuit

A turbine blade has been adapted (**Sheldrake and Ainsworth, 1995**) to carry a leading edge, mid-height, two sensor hot-wire probe, Figure 2, to enable the free-stream rotor relative inlet Mach number and whirl angle to be determined. The hot-wire probe takes the role of a "plug" which may be inserted into the turbine blade. This allows the hot-wire elements to be replaced relatively simply, by removing the probe from the blade. The probe is controlled by an anemometer circuit (**Sheldrake and Ainsworth, 1994a**) contained within the turbine shaft, Figure 3. Each anemometer, Figure 4, consists of three electrically independent anemometer pods allowing a maximum of three hot-wires to be operated at any one time. The output signals from the anemometers connect with the stationary frame of reference via slip rings mounted on the end of the turbine shaft.

Hot-wire Probe Calibration

The fluid properties that exist at rotor inlet, in the relative frame of reference, are shown below in Table 2. The blade mounted dual sensor hot-wire probe is calibrated for velocity within the working section of the Oxford Rotor facility, Figure 5, using a compact calibration nozzle, operated with the working section pressurised to the rotor inlet static pressure. Geometrical constraints within the working

Total Pressure	5.05×10^5 Pa
Static Pressure	4.43×10^5 Pa
Total Temperature	327 K
Static Temperature	316 K
Static Density	5.14 kg/m^3
Inlet Mach Number	0.4

Table 2

section mean that it is not possible to position the calibration nozzle so that it can calibrate the dual hot-wire probe over a range covering the expected pitch-wise whirl angle variation, namely ±25°. This difficulty is overcome by using an analytical expression to represent the yaw response of hot-wire elements. The technique allows a velocity calibration, performed in line with the axis of the probe (at zero yaw angle) to be combined with a yaw calibration, which together give a two-dimensional probe calibration. The yaw calibration determines two yaw coefficients which characterise the angular response of the probe. These are obtained from data acquired in a variable density flow calibration facility (**Sheldrake, 1995**). Briefly, this consists of a 50 mm diameter nozzle in which the hot-wire probe may be accurately positioned in yaw by a stepper motor controller. An upstream throttle allows control of the nozzle exit Mach number, whilst the total pressure is regulated by a downstream valve.

***In situ* Hot-wire Velocity Calibration**

The calibration nozzle is positioned within the working section of the Oxford Rotor facility, Figure 5, with the nozzle exit plane approximately one diameter away from the plane containing the hot-wire sensors and with the nozzle axis aligned with the probe's axis. The working section is then pressurised

to the design rotor inlet static pressure of 443 kPa. A small high pressure (700 kPa) reservoir supplies air to the calibration nozzle, via a bulkhead connection through one of the cassettes, and the pressure drop that occurs between the nozzle and the working section is measured by a National piezoresistive pressure transducer. This is used to calculate the nozzle exit Mach number, the calibration ranging from Mach 0.3 to 0.5. The total temperature of nozzle exit flow is estimated by a K-type thermocouple located at the entrance to the settling chamber inside the nozzle.

The highest nozzle exit Mach number condition (M = 0.5) is established initially, a valve in the reservoir supply line is then closed allowing the air pressure in the small reservoir to drop as a function of time. This has the effect of steadily reducing the pressure drop across the nozzle and thereby decreasing the nozzle exit Mach number. The output voltages from the anemometers, the raw pressure drop and total temperature signals are conditioned by low pass filters before being digitised by a transient recorder, sampling at 100 Hz. The nozzle pressure drop and total temperature traces obtained from a typical dual hot-wire probe velocity calibration are shown in Figures 6 and 7. The accompanying graphs, Figures 8 and 9 show the output voltages from the "tip" and "root" hot-wires from the dual sensor probe. The assignations "tip" and "root" refer to the wire closest to the tip and root of the turbine blade respectively, Figure 10. A heat balance according to the simple power law

$$E^2 = A + B V_{eff}^n \qquad 1$$

is applied to the calibration data where V_{eff} is the effective cooling velocity. The hot-wire voltages are corrected to 289 K using the linear correction method (**Kanevce and Oka, 1973**) to compensate for any variation in the total temperature of the fluid during calibration. A least squares analysis is used to calculate the optimum values of A, B and n, the accuracy of the curvefit being evaluated from **Bruun, *et al*, 1990b**. It was found that all calibrations fell within the 0.1 to 0.3% error range.

Angular Calibration

As mentioned above, the geometrical constraints present within the working section prevent the calibration nozzle being used to calibrate the hot-wire probe over the required range of yaw angles. The use of the effective cooling velocity concept provides a convenient solution to this problem. Of the numerous possible analytical expressions for the yaw response the most commonly used is that attributable to **Jorgensen, 1971**, viz

$$V_{eff} = \tilde{V} (\cos^2\alpha + k^2 \sin^2\alpha)^{0.5} \qquad 2$$

where k^2 is the yaw coefficient, $\tilde{V}$ is the magnitude of the incident velocity vector and α is the yaw angle, Figure 10. This analytical expression is often chosen because it gives the smallest errors in axial and tangential components of velocity over the full calibration range and it is reasonably insensitive to the exact determination of the individual separation yaw angles for the two wires (**Bruun, *et al*, 1990a**). The yaw coefficient may be regarded as an aerodynamic factor that is specific to a particular probe geometry - once k^2 has been determined it should remain constant even after renewing the sensing element.

The yaw coefficients for each wire of the dual sensor probe are obtained from data acquired in a variable density flow calibration facility. A single velocity calibration was performed in line with the axis of the probe, $\alpha = \bar{\alpha}$, which defined A, $B(\cos^2\bar{\alpha} + k^2\sin^2\bar{\alpha})^{\frac{n}{2}}$ and n for each wire. A yaw calibration

was then carried out over $\theta = \pm 25.2°$ in 1.8° steps for a constant nozzle exit Mach number of 0.40 and a total pressure of 500 kPa. These conditions being representative of the rotor relative environment at the design point. The following ratio, E^{*2}, may then be calculated for each yaw angle and sensor

$$E^{*2} = \left[\frac{E_\theta^2 - A}{E_{\bar{\alpha}}^2 - A}\right]^{\frac{2}{n}} = \frac{\cos^2\alpha + k^2 \sin^2\alpha}{\cos^2\bar{\alpha} + k^2 \sin^2\bar{\alpha}} \qquad 3$$

This expression can be rearranged into the form $y = mx$, such that

$$E^{*2} - 1 = (1 - k^2)\,[E^{*2} \sin^2\bar{\alpha} - \sin^2\alpha] \qquad 4$$

A least squares curvefit was then applied to the calibration data to determine the gradient and hence yaw coefficient for each sensor. The results are shown in Figure 11. The tip and root wires are clearly well matched, indicated by the similar yaw coefficients, $k^2_{tip} = 0.012$ and $k^2_{root} = 0.014$. Similar figures have been observed by **Jorgensen, 1971**, **Bremhorst, 1981** and **Bruun, *et al*, 1990b**. The values for k^2 can then be substituted into equation 2 and the result substituted into equation 1 to find B for each wire.

The measured effective cooling velocities for the tip and root wires must be transformed into axial and tangential velocity components with respect to the probe coordinate system, Figure 10. From this reference point the rotor relative inlet Mach number and whirl angle can then be calculated. A modified version of the sum-and-difference equations are used here, in preference to the simple sum-and-difference equations (**Bradshaw, 1971**) which allow different yaw coefficients, for the tip and root wires, to be accounted for, viz

$$U = \frac{\dfrac{V_{tip}\, g_{root}(\bar{\alpha})}{f_{tip}(\bar{\alpha})} + \dfrac{V_{root}\, g_{tip}(\bar{\alpha})}{f_{root}(\bar{\alpha})}}{g_{tip}(\bar{\alpha}) + g_{root}(\bar{\alpha})} \qquad 5$$

$$V = \frac{\dfrac{V_{root}}{f_{root}(\bar{\alpha})} - \dfrac{V_{tip}}{f_{tip}(\bar{\alpha})}}{g_{tip}(\bar{\alpha}) + g_{root}(\bar{\alpha})} \qquad 6$$

where the two yaw functions

$$f(\bar{\alpha}) = (\cos^2\bar{\alpha} + k^2 \sin^2\bar{\alpha})^{0.5}$$

$$g(\bar{\alpha}) = \frac{(1 - k^2)\cos^2\bar{\alpha}\, \tan\bar{\alpha}}{\cos^2\bar{\alpha} + k^2 \sin^2\bar{\alpha}} \qquad 7$$

must be evaluated using the respective yaw coefficients.

The Rotor Relative Inlet Flow-field: Experimental Results and CFD Prediction

The high bandwidth data obtained from the dual sensor hot-wire probe enables the pitch-wise variation in rotor relative inlet Mach number and whirl angle to be determined. A representative example of the rotor relative inlet Mach number and whirl angle distribution measured by the dual sensor hot-wire probe is shown in Figures 12 and 13. These data are plotted together with the outputs from a single and a 36 line shaft encoder mounted on the turbine shaft. The single line encoder determines the angular position of the turbine blade row, whereas the 36 line disc is used to define the wake passing frequency in the rotor relative frame of reference (there being 36 nozzle guide vanes). A characteristic structure repeating at the rotor relative blade passing frequency (approximately 5 kHz) is very evident in both Figures. Although this pattern can easily be recognised, slight passage-to-passage variations exists in the aerodynamic characteristics of each stator passage. Perhaps more meaningful then is the phase-average waveform, Figures 14 and 15. The rotor relative inlet Mach number obtained from the single sensor probe is shown in Figure 16, along with the phase-averaged waveform, Figure 17, for comparison. Clearly there is great similarity between the derived inlet Mach number from the single and dual sensor probes in terms of characteristic structure and mean signal level, which is a very reassuring result. Evidently, the pitch-wise Mach number signature from the dual hot-wire probe, Figure 12, is slightly less clear than that from the single sensor probe. This is probably due to either the physical separation of the hot-wire elements (*id est* the measurements are not made in exactly the same plane) or to the processing technique used to transform the anemometer output voltages into the flow vector. (Because the voltages from both of the two hot-wires are combined to give the magnitude of the flow vector, rather than this being obtained from a single element, the derived result will inevitably incorporate noise and spurious signals from both sources).

Heuristically, the narrow sharp drop in rotor relative inlet Mach number could be said to correspond to the hot-wire probe traversing the near wake shed from an upstream stator blade. This was confirmed with reference to the geometry of the facility and the output signal from the one line shaft encoder. At the centre-line of the wake region the Mach number is reduced to about 80% of the time-averaged mean value.

Turning to the variation in rotor relative inlet whirl angle with stator pitch, Figure 15. The position of an NGV wake can be identified with each sharp drop in whirl angle. The wake represents a region of reduced Mach number, where the absolute NGV exit Mach number will be lower than the free-stream value. Therefore, there will be a corresponding drop in the rotor relative inlet Mach number as the blade whirl Mach number remains constant. The rotor relative inlet whirl angle must fall accordingly, *ipso facto*. Similarly the drop in inlet Mach number that occurs at approximately the mid-passage position corresponds to a drop in inlet whirl angle.

The origin of the drop in rotor relative inlet Mach number and whirl angle that occurs between concurrent NGV wakes is caused by a region of high free-stream static pressure in the proximity of the NGV trailing edge on the suction surface side. In this region the flow is being rapidly accelerated and the free-stream Mach number is just sonic. Weak, normal, shock waves propagate from the trailing edge region, on the suction surface of the aerofoil, causing the local Mach number to fall due to the increase in static pressure, Figure 18. Schlieren photography taken by **Nicholson, 1981** in a linear cascade of a similar vane profile reveal evidence of normal shock waves along the surface of the aerofoil, close to the trailing edge, the exact location being dependent upon the isentropic exit Mach number and Reynolds

number.

The computational code UNSFLO (**Giles, 1988**) has been used to provide a prediction of the unsteady the rotor relative flow-field for comparison with the experimental data. UNSFLO is a two-dimensional, unsteady viscous solver specifically designed to analyse viscous and potential rotor/stator interaction. It has recently been used for both unsteady heat transfer (**Korakianitis, 1993**) and surface pressure (**Moss, *et al*,1995**) prediction. Good agreement was obtained between experiment and prediction.

For the present study UNSFLO was configured with a grid resolution of 120x30 points for each of the stator and rotor passages. The solution obtained is based upon the operating point of the Oxford Rotor. The UNSFLO prediction for the rotor relative inlet Mach number and whirl angle are show in Figures 19 and 20, together with the phase-averaged results from the dual sensor hot-wire probe. In terms of characteristic structure there is an excellent correlation between the rotor relative inlet Mach number from UNSFLO and experiment. The width of the wakes shed from the upstream stator blades are accurately predicted by UNSFLO as is the position of the drop in Mach number that occurs between concurrent wakes. With the exception of the wake region, where UNSFLO underpredicts the Mach number deficit by approximately 25%, the comparison between the signal perturbation is excellent. However, the time-averaged Mach number from UNSFLO is approximately Mach 0.08 (20%) below the measured level from the hot-wire probe. It is possible that some adjustment to the throat areas or hade may correct this for future calculations.

The UNSFLO prediction for the rotor relative inlet whirl angle is also in good agreement with the experimental value. UNSFLO predicts a time-mean whirl angle approximately 4° higher than the hot-wire result with a slightly larger variation in whirl angle through the wake region and a lower perturbation in-between.

Conclusions

The use of blade mounted hot-wires has been shown to be of considerable importance as an investigative tool for the rotor relative frame of reference. This novel technique has provided a direct measurement, at high bandwidth, of the pitch-wise rotor relative inlet Mach number and whirl angle distributions present in a high speed turbine facility, thereby adding to our understanding of the complex rotor relative flow-field.

The construction of the hot-wire blades as a whole, used in conjunction with the "in-shaft" anemometer module and the *in situ* calibration nozzle has proved to be particularly successful. The ability to remove and replace the probes from the turbine blades with comparative ease, using the plug and socket arrangement, has lent itself to the technique.

The agreement obtained between the single and dual sensor hot-wire probes and the CFD prediction is seen as being most encouraging.

Acknowledgements

The authors would like to acknowledge the DRA Pyestock and Rolls-Rolyce plc for their support and permission to publish this paper. Thanks are also due to Kevin Grindrod for his enthusiasm in running the ILPT facility.

References

Ainsworth, R.W., Schultz, D.L., Davies, M.R.D., Forth, C.J.P., Hilditch, M.A., Oldfield, M.L.G. and Sheard, A.G., "A Transient Flow Facility for the Study of Thermofluid-Dynamics under Engine Representative Conditions". A.S.M.E. Paper 88-GT-144, 1988.

Brawshaw, P. An Introduction to Turbulence and its Measurement. Pergamon Press, Oxford, 1971.

Bruun, H.H., Nabhani, N., Al-Kayiem, H.H., Fardad, A.A., Khan, M.A. and Hogarth, E. Calibration and analysis of *X* hot-wire prove signals. *Meas. Scie. Technol.*, Vol. 1, pp. 782-785. 1990a.

Bruun, H.H., Nabhani, N., Farad, A.A. and Al-Kayiem, H.H., "Velocity Component Measurements by Cross Hot-wire Anemometry". Journal of Measurement Science and Technology, pp 1314-1321, 1990b.

Doorly, D.J. and Oldfield, M.L.G., "Simulation of Wake Passing in a Stationary Turbine Rotor Cascade", Journal of Propulsion, pp 316-318, Vol. 1, No. 4, July 1985.

Giles, M.B. Calculation of unsteady wake rotor interaction. *AIAA J. of Prop. and Power, Vol. 4*, pp. 356-362, 1988.

Jorgensen, F.E., "Directional Sensitivity of Wire and Fibre-film Probes". DISA Information No. 11, pp 31-37, 1970.

Kanevce, G. and Oka, S. "Correcting Hot-wire Readings for Influence of Fluid Temperature Variations". DISA Information No.15, pp 21-24, 1973.

Korakianitis, T. On the propagation of viscous wakes and potential flow in a axial turbine cascades. *Journal of Turbomachinery*, Vol. 115, pp.118-127, 1993.

Morel, T. "Comprehensive Design of Axisymetric Wind Tunnel Contractions". Journal of Fluids Engineering, ASME Trans, pp 225-233, 1975.

Moss, R.W., Sheldrake, C.D. and Ainswoth, R.W. Unsteady pressure and heat transfer measurements on a rotating blade surface in a transient flow facility. *AGARD*, 1995.

Nicholson, J.H., "Experimental and Theoretical Studies of the Thermal Performance of Modern Gas Turbine Blades". D.Phil. Thesis, University of Oxford, 1981.

Perry, A.E. and Morrison, G.L., "A Study of Constant-temperature Hot-wire Anemometry". Journal of Fluid Mechanics, Vol. 47, Part 3, pp 577-599, 1971.

Sheldrake, C.D. "Unsteady Effects in the High Pressure Stage of a Model Gas Turbine". D.Phil. Thesis, University of Oxford, 1995.

Sheldrake, C.D. and Ainsworth R.W., "Hot-wire Anemometry Techniques on Rotating Turbine Experiments". 12th Symposium on Measuring Techniques on Transonic and Supersonic Flow in Turbomachines, Prague, 1994.

Sheldrake, C.D. and Ainsworth, R.W. The use of hot-wires applied to aerodynamic measurements in a model turbine stage. *1st European Conference on Turbomachinery Fluid Dynamic and Thermodynamic Aspects*, pp. 149-173, Nuremburg, March 1995.

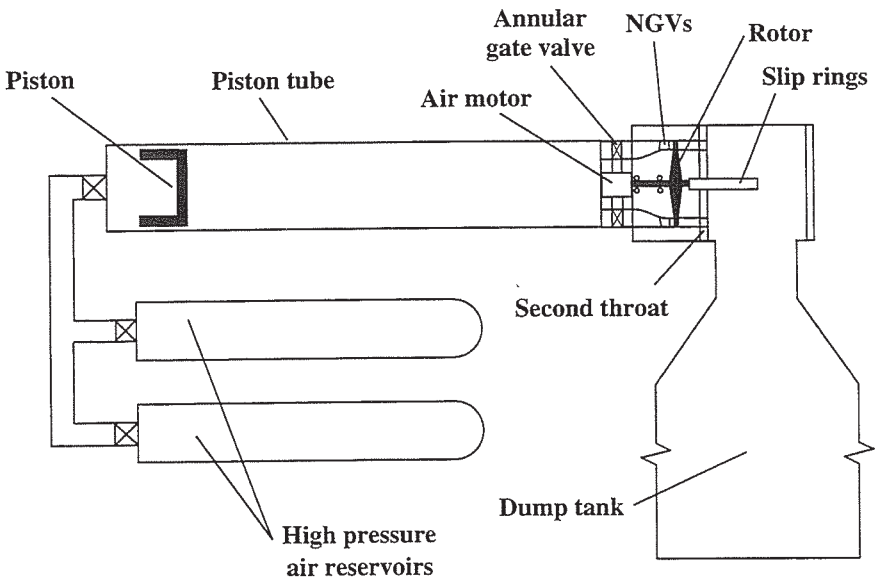

Figure 1 Schematic of the ILPT

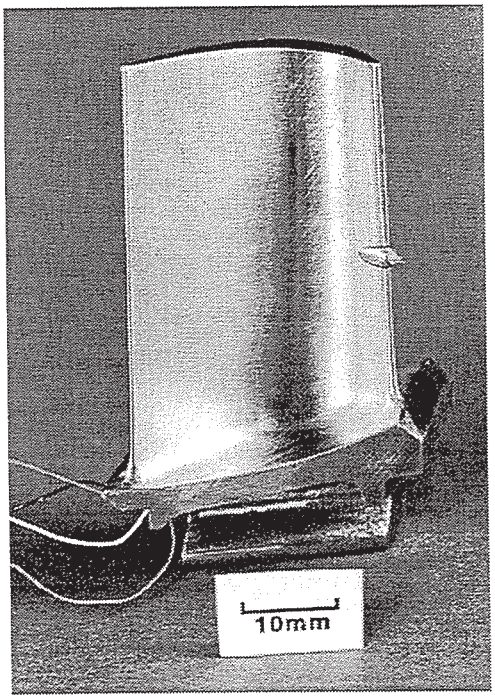

Figure 2 View of the adapted Turbine Blade
with the Dual Sensor Hot-wire Probe

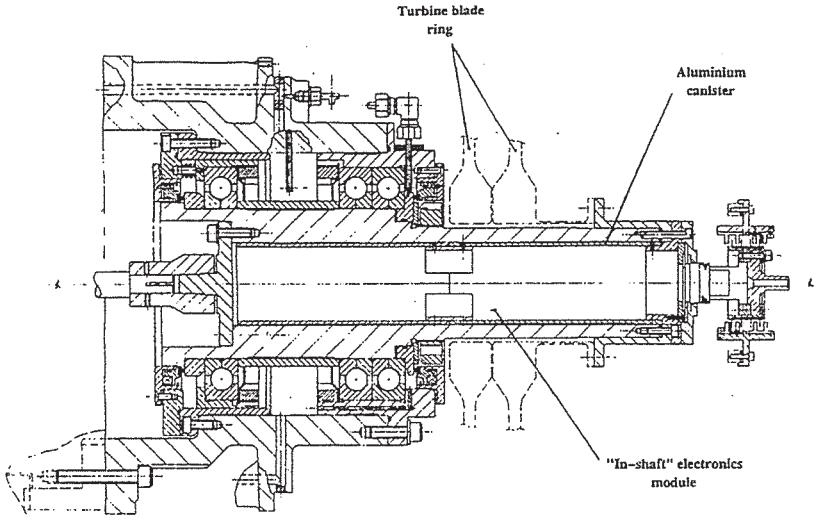

Figure 3 Schematic of the Oxford Rotor Showing the Position of the "In-shaft" Electronics Module

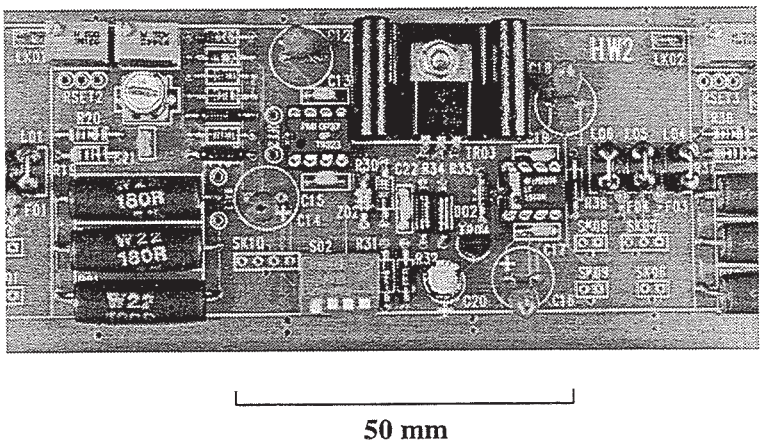

Figure 4 View of the in-shaft Hot-wire Anemometer PCB

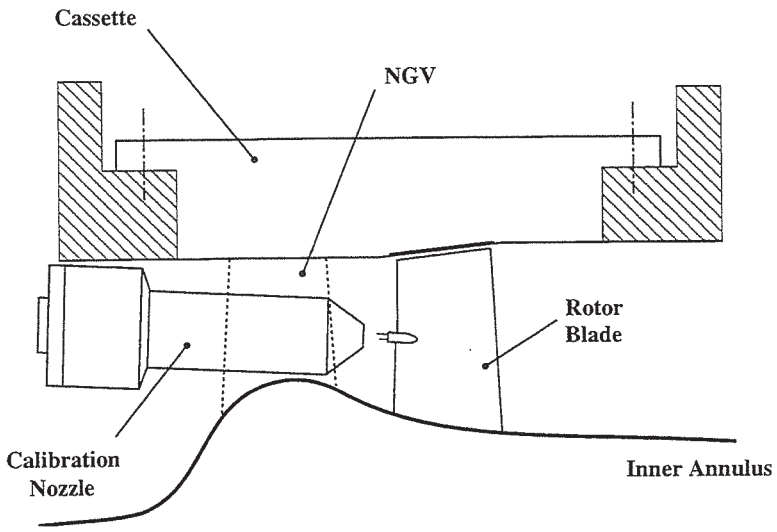

Figure 5 Schematic showing the Position of the Calibration Nozzle

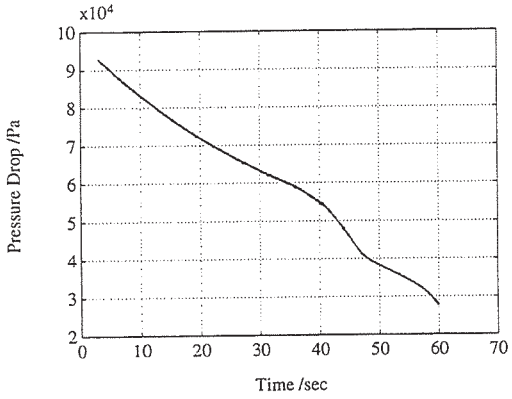

Figure 6 Calibration Nozzle Total Pressure

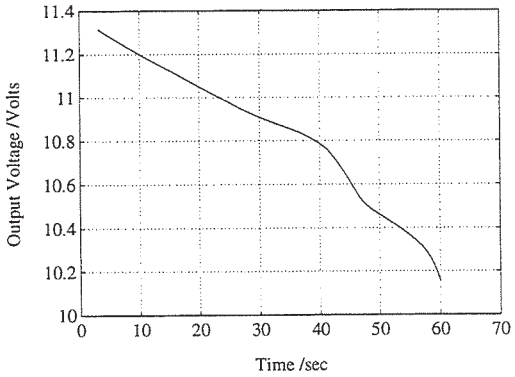

Figure 7 Calibration Nozzle Total Temperature

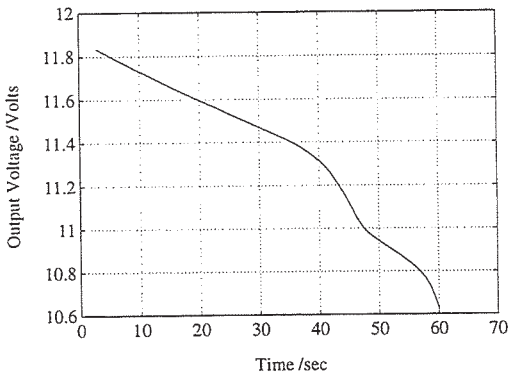

Figure 8 Tip Hot-wire Calibration

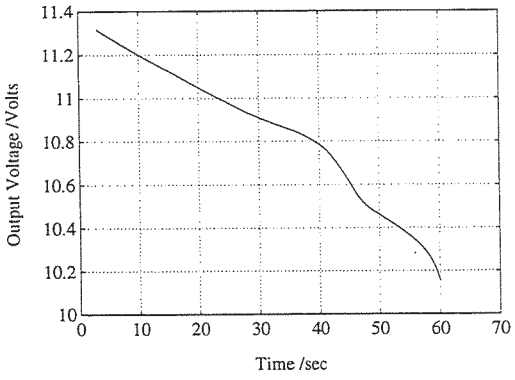

Figure 9 Root Hot-wire Calibration

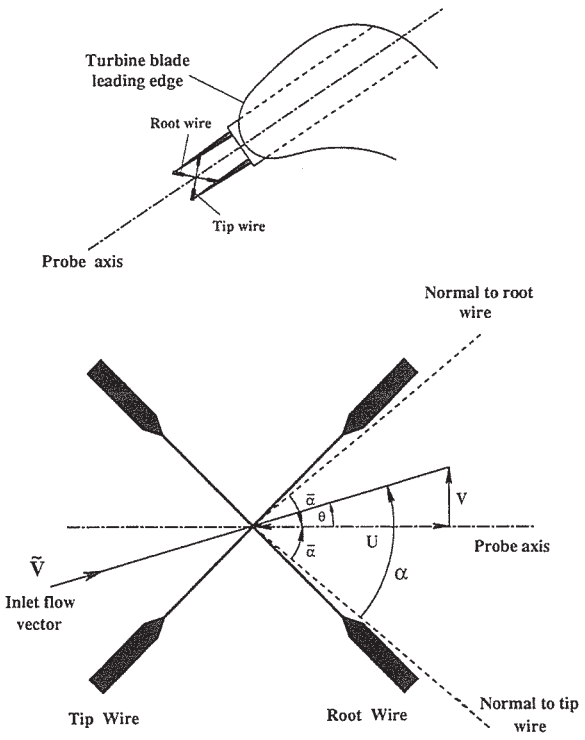

Figure 10 Dual Sensor Hot-wire Probe Geometry

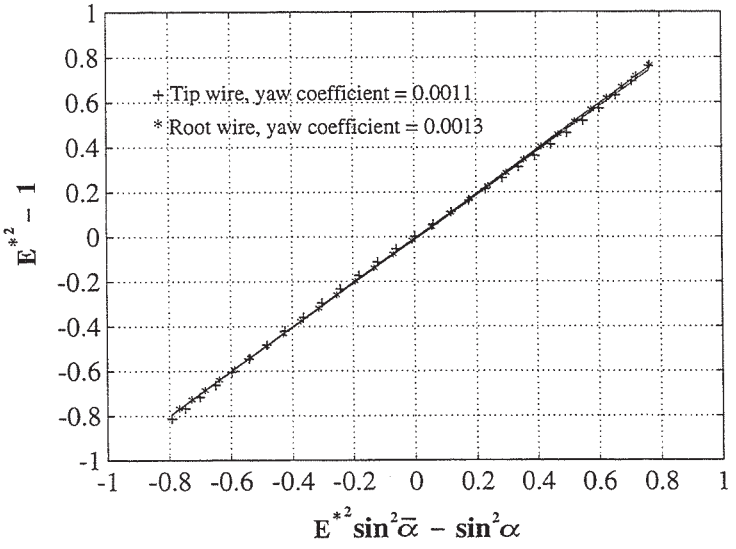

Figure 11 Evaluation of the Yaw Coefficients for the Dual Sensor Hot-wire Probe

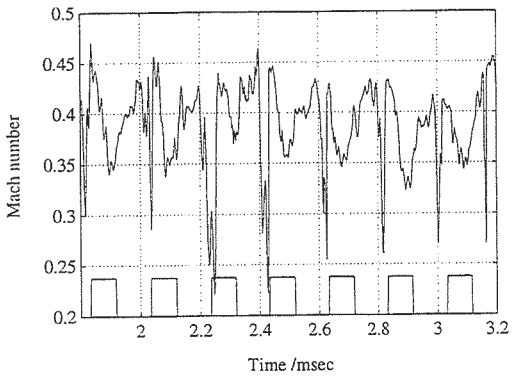

Figure 12 Rotor Relative Inlet Mach number: Dual Sensor Probe

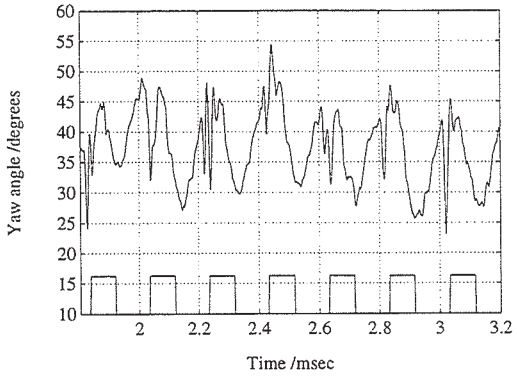

Figure 13 Rotor Relative Inlet Whirl Angle: Dual Sensor Probe

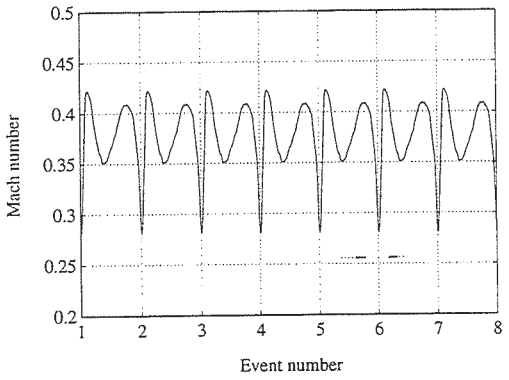

Figure 14 Phase Averaged Rotor Relative Inlet Mach number: Dual sensor probe

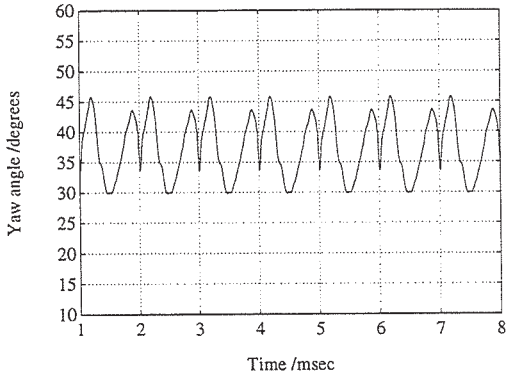

Figure 15 Phase Averaged Rotor Relative Inlet Whirl Angle: Dual Sensor Probe

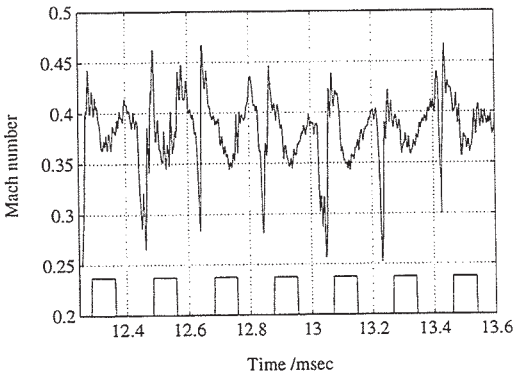

Figure 16 Rotor Relative Inlet Mach number: Single Sensor Probe

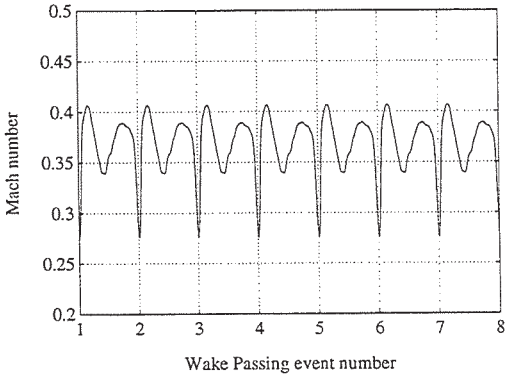

Figure 17 Phase Averaged Rotor Relative Inlet Mach number: Single Sensor Probe

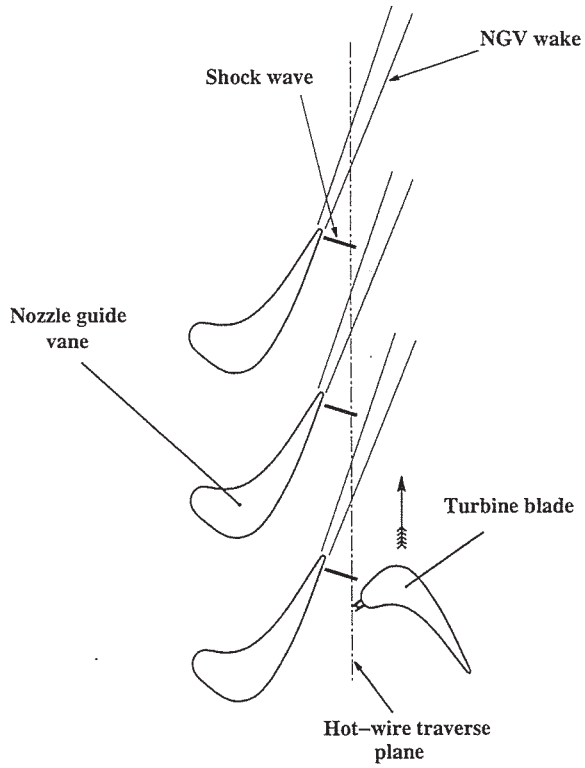

Figure 18 Shock Interaction in Rotor Relative Inlet Flow-field

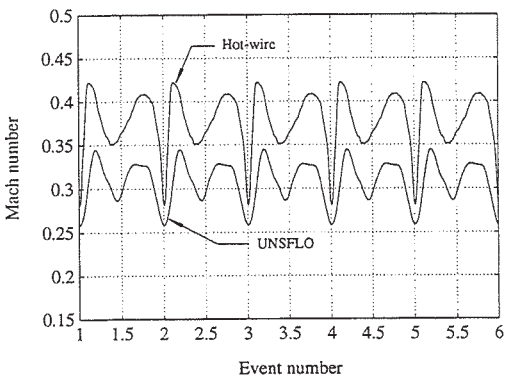

Figure 19 Comparison Between UNSFLO and Hot-wire Measurement of the Resultant Rotor Relative Inlet Mach Number

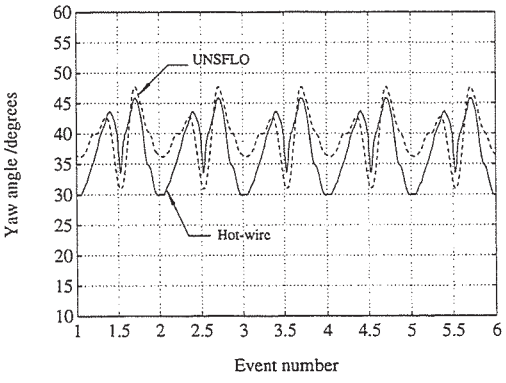

Figure 20 Comparison Between UNSFLO and Hot-wire Measurement of the Rotor Relative Inlet Whirl Angle